Broken symmetries in the crystalline and magnetic structures of γ-iron

M. Marsman and J. Hafner

Institut für Materialphysik and Center for Computational Material Science, Universität Wien, Sensengasse 8, A-1090 Wien, Austria

It is by now well established that in antiferromagnetic γ-Fe, stabilized in the form of precipitates in a Cu matrix or by epitaxial growth on an appropriate substrate, magnetic and/or crystalline symmetries are broken. Little is known, however, on the physical effects driving the symmetry reduction, and on the interplay of crystalline and magnetic symmetry breaking. We have used a recently developed unconstrained vector-field description of noncollinear magnetism, implemented in an *ab initio* spin-density-functional code, to search for the magnetic and crystalline structure of γ-Fe, stabilized by different types of constraints. We show that in near face-centered-cubic γ-Fe, stabilized by three-dimensional constraints, the magnetic ground state is a spin-spiral with propagation vector $\vec{q} = 2\pi/a \times (0.2,0,1)$ at an equilibrium atomic volume of $\Omega = 10.63$ Å^3, very close to the propagation vector $\vec{q}_{\mathrm{exp}} = 2\pi/a \times (0.1,0,1)$, determined experimentally, but at considerably lower volume than the atomic volume of the γ-Fe precipitates in Cu on which the experiments were performed ($\Omega = 11.44$ Å^3). At these larger volumes our calculations predict an helical spin solution at $\vec{q} = 2\pi/a \times (0,0,0.6)$ to be the ground state. Epitaxially stabilized γ-Fe is found to be unstable against both tetragonal distortion as well as monoclinic shear deformation, and the structural distortions suppress the formation of spin-spiral states, in agreement with experimental observations on Fe/Cu(100) films.

I. INTRODUCTION

Among the $3d$ elements showing itinerant magnetism, iron occupies a unique role. In the Slater-Néel curve (see, for instance, Ref. 1) representing the exchange interaction as a function of the interatomic distance, Fe falls close to the node separating the antiferromagnetic metals Cr and Mn with a nearly half-filled d band from the strong ferromagnets Co and Ni with a nearly full band. Body-centered cubic (bcc) α-Fe has a nearest neighbor distance sufficiently large to stabilize ferromagnetism, but the increasing slope of the Slater-Néel curve leads to strong magnetovolume effects in weakly ferromagnetic α-Fe contrasting the behavior of the strong ferromagnets Co and Ni. Due to the higher packing-density of face-centred cubic (fcc) γ-Fe, the nearest-neighbor distance is small enough so that γ-Fe should be antiferromagnetic in analogy to Mn and Cr. In amorphous Fe, the first peak of the pair-correlation function falls close to the zero in the Slater-Néel curve, leading to a competition between ferromagnetic and antiferromagnetic exchange interactions. Depending on the mean nearest-neighbor distance between the Fe atoms, amorphous alloys with a second non-magnetic metal or a metalloid (the addition of a second element is necessary to allow the formation of a metastable amorphous phase at not too high quenching rates) will show asperomagnetism or speromagnetism.[2–4]

The investigation of antiferromagnetic γ-Fe is complicated by two facts: (i) The fcc phase is stable only in the temperature interval from $T = 1173$ K and $T = 1660$ K, i.e., far above the expected Néel temperature. (ii) As antiferromagnetic ordering breaks the cubic symmetry, the paramagnetic to antiferromagnetic transition is eventually coupled to a structural distortion.

The situation could be similar to that observed in α- and γ-Mn—in both cases the symmetry of the cubic paramag-

netic phase is reduced to tetragonal in the antiferromagnetic phase.[5–8] The coexistence of tetragonally distorted, type-I antiferromagnetic fcc Mn with α-Mn and its complex crystalline and noncollinear magnetic structures is indeed a striking demonstration of the complex structure-property relationship in the itinerant antiferromagnets. A further example is the instability of bcc type-I antiferromagnetic Cr to the formation of a long-period spin-density-wave coupled to a strain-wave of half wavelength.[9,10]

Experimentally, γ-Fe has been produced mainly by two different techniques. (i) Annealing of dilute alloys of Fe in fcc Cu leads to the formation of precipitates with the same structure as the parent lattice. (ii) The epitaxial growth of ultrathin Fe layers on Cu(001) or Cu(111) substrates is known to stabilize the fcc structure up to a certain critical film thickness.

The structural and magnetic properties of γ-Fe precipitates in Cu have been studied extensively by Tsunoda *et al.* using various techniques.[11–17] It was shown that both the crystalline and magnetic structures depend quite crucially on the diameter of the precipitates (which is in turn a function of the thermal history of the sample). For particle sizes up to 150 Å, below a Néel temperature of 50 K, a simple type-I antiferromagnetic structure with a low magnetic moment ($m_{\mathrm{Fe}} \leq 1 \mu_B$) is formed. The phase transition is second order, the crystal structure is unchanged in this antiferromagnetic γ-A phase down to the lowest temperatures. For precipitates with diameters ranging between 150 and 1500 Å, the magnetic phase transition observed at $T \sim 50-70$ K is first order and coupled to a structural phase transition. In the antiferromagnetic γ-B phase, the fcc lattice contracts along the c axis, in the c plane the atomic positions are modulated by a long-period transverse wave propagating along the [110] direction. The wavelength of the lattice modulation varies with the diameter of the precipitates. The magnetic structure is a

helical spin-wave with the periodicity of the lattice modulation. The increase of the Néel temperature compared to the γ-A phase signals that the lattice modulation stabilizes the antiferromagnetism. For precipitates with a still larger diameter (γ-C phase) the Néel temperature and the structural phase-transition temperature are not well defined, they show a broad distribution correlating quite well with the distribution of the measured lattice spacings. This indicates that the full coherence with the Cu matrix has been lost and that the semicoherent γ-Fe precipitates are surrounded by many interface dislocations. Both the structural and magnetic phase transitions are coupled rather strongly to alloying and volume effects: Alloying of Fe with Co strongly suppresses the structural phase transition and lowers the Néel temperature while alloying with Cr increases the transition temperature for both the structural and magnetic transitions (which remain strongly coupled). This is related to two effects: on one hand, alloying with Co stabilizes the fcc phase, whereas it is destabilized by addition of Cr, on the other hand, Co decreases the lattice constant of the precipitates (and hence increases the lattice mismatch and reduces the transition temperatures), whereas Cr acts in the opposite direction. However, the situation is extremely complex: for precipitates in a dilute alloy of Cu with Au where the lattice mismatch is also increased, an increase of the transition temperature has been observed.

Ultrathin γ-Fe films grown on Cu(001) also show a very complex structural and magnetic phase diagram.[18–25] Films with up to 3–4 monolayers (ML) are ferromagnetic, the structure is tetragonally distorted fcc (Refs. 19–21) and shows a considerable three-dimensional lattice modulation[22] with (1×4) or (1×5) periodicity (region I). At thicknesses ranging from about 4 to 11 ML (region II) the Fe films have been characterized as fcc "on average" and antiferromagnetic,[23–25] with a small net moment due to a ferromagnetic coupling of the enhanced moments in the surface and subsurface layers, varying in a nonmonotonous way with the film thickness. For films with about 6 ML a (1×2) reconstruction has been reported. The magnetic ordering transition has been found to be rather complex: the temperature dependence of the magnetization is characterized by a steep increase at the Curie temperature T_c and a second steep increase at a lower temperature T_e which has been interpreted as the effective ordering temperature of the antiferromagnetic underlayers. Both the nonmonotonous variation of magnetization with thickness and the two-step magnetic transition have been tentatively assigned to the formation of a helical spin-wave in the deeper layers,[26] in analogy with the modulated magnetic structure of the γ-Fe precipitates. Films thicker than about 10–11 ML transform to a bcc structure.

Very recently investigations of the structure of ultrathin γ-Fe films using scanning tunneling electron microscopy have added to the complexity of this picture.[27] In regime II it was found that bcc nucleation centers appear as long needle-like crystals which had been described also in earlier studies.[28] Within the needles, atomic rows are tilted with respect to the underlying fcc lattice but appear to be perfectly lattice matched on both sides. The tilt angle is smaller than the 19.5° corresponding a bcc overlayer on a fcc substrate. In regime I, a large portion of the surface of the film is covered by a zigzag-pattern with (1×n) periodicity $n=4$–6. In analogy with the needles found in the thicker films, this structure has been described as consisting of stripes with a local bcc structure. All structures can be described as resulting from a monoclinic shearing of the fcc lattice by $\pm 14°$ such that the local atomic configuration is very similar to that of a (110) bcc film in the Pitsch orientation[29] with respect to the fcc (001) substrate. Films with about 3 ML, i.e., in the ferromagnetic regime I show the highest content of "bcc-like" stripes—this has been interpreted as representing a strong correlation between film structure and magnetism. However, there is no evident correlation between these short-period reconstructions and the long-period modulations observed in γ-Fe precipitates beyond the fact that both distortions are coupled to the magnetic structure.

Altogether the results on both precipitates and ultrathin films indicate a pronounced tendency of antiferromagnetic fcc Fe to form distorted (modulated) crystalline and magnetic structures, with the details of this modulation depending in a crucial way on the constraints (two or three dimensional) stabilizing the near-fcc symmetry. The correct theoretical prediction of the structural and magnetic ground state of Fe proved to be a very difficult task: early first-principles calculations performed in the local-spin-density approximation (LSDA) found the nonmagnetic hexagonal lose-packed phase (ϵ-Fe) to be lower in energy, only the inclusion of generalized gradient corrections to the exchange-correlation functional led to the correct result of a ferromagnetic bcc ground state (see, e.g., Ref. 30 and further references cited therein).

LSD calculations performed in the generalized-gradient approximation (GGA) also considerably contributed to clarify the structural and magnetic phase diagram of γ-Fe/Cu(001) films.[31–37] The calculations explain the stability of the ferromagnetic state in regime I as resulting from the surface-induced enhanced magnetic moments and their tetragonal distortion as resulting from a magnetovolume effect. In the regime II AFM high-moment ($m_{Fe}\sim 2\mu_B$) structures are predicted, with a bilayer sequence ($\uparrow\uparrow\downarrow\downarrow\cdots$) of the spin orientations for films with an even number of ML. Interlayer distances between FM coupled layers are expanded, AFM coupling leads to contracted spacings so that the structure is fcc on average. In the course of these investigations it was also found that bulk γ-Fe is instable against tetragonal shear in all magnetic phases.[35,36] The most recent work[35,37] has demonstrated that the three-dimensional "sinusoidal" distortion reported on the basis of LEED experiments and the stripe patterns with various periodicities observed in the STM are in fact identical and accurately described by DFT calculations. In the course of these investigations, an unexpected fundamental instability of bulk γ-Fe not only against tetragonal, but also against monoclinic shearing was discovered. The shearing angle predicted for bulk γ-Fe corresponds exactly to the angle calculated for the stripe domains on the surface of the ultrathin films and measured in the STM experiments. Hence the stripe pattern can be considered as arising from the formation of nanotwins of the

stable bulk phase. In contradiction to the suggestion of Qian *et al.*[26] it was found that helical spin waves are unstable in ultrathin γ-Fe films and that the observed stepwise increase of the magnetization at decreasing temperature is better described in terms of decoupled phase transitions at the surface and in the deeper layers.[38,39] Only collinear magnetism exists in the thin Fe films.

A number of attempts have been made to investigate the spin-spiral magnetism in bulk γ-Fe,[40–47] assuming an ideal fcc lattice. All early calculations using the LSDA (Refs. 40–42) confirmed the spin-spiral ground-state of γ-Fe, but predicted a wave vector of $\vec{q} = 2\pi/a \times (0,0,0.6)$ instead of the experimentally determined $\vec{q}_{\exp} = 2\pi/a \times (0.1,0,1)$ and agreed on a strong sensitivity of the energy difference between the spin-spiral state relative to the commensurate antiferromagnetic structure on the atomic volume. Körling and Ergon[43] showed that the use of the GGA leads to a spin spiral with $\vec{q} = 2\pi/a \times (0.5,0,1)$, demonstrating a strong effect of the gradient corrections, but unfortunately also in disagreement with experiment. Bylander and Kleinman[44] added a "spin stiffness" correction to the exchange-correlation functional, but did not succeed in stabilizing a spin spiral with the observed wave vector. Various complex collinear antiferromagnetic configurations were investigated by James *et al.*,[45] Herper *et al.*,[46] and Spišák and Hafner.[35,37,38] All studies agree that a bilayer antiferromagnetic structure is more stable than a single-layer antiferromagnetic configuration. So far all calculations were based on the assumption of a fixed spin-quantization axis within atomic spheres—the direction of magnetization changes discontinuously when passing from one sphere to the next. In a recent paper Knöpfle *et al.*[47] used a *modified* augmented spherical wave (ASW) method allowing also for an intra-atomic noncollinearity of the spins. For lattice constants smaller than about 3.57 Å they found a wave vector $\vec{q} = 2\pi/a \times (0.15,0,1)$ for the ground state of the spin spiral in agreement with experiment, although at a slightly too small lattice constant. Comparing this result with the earlier calculations leads to the conclusion that the full-potential corrections to the spin density are essential for obtaining the correct spiral wave vector. However, it is well known that the ASW method [and the closely related linearized muffin-tin-orbital (LMTO) technique likewise] tends to overestimate the equilibrium density. Hence it remains unclear whether at the density of Fe precipitates in Cu, the helical state with the correct wave vector will represent the true ground state. Very recently, for the experimental density of γ-Fe a similar result was published by Luo and Yao,[48] although the technical details of this work remain a bit obscure.

However, so far no attempt has been made to investigate the influence of a broken cubic symmetry on the stability of the helical spin wave. The aim of our work is to complete the investigation of the structure-property relationship in γ-Fe by investigating the correlation between the broken crystalline and magnetic symmetries. We shall first extend the structural investigations of γ-Fe in various collinear phases, turn then to the question of the stability of a helical spin state in the cubic phase of varying density and finally investigate the cross-correlations between tetragonal distortions, orthorhombic distortions, monoclinic shearing deformation, and spin-wave magnetism.

II. METHODOLOGY

Our calculations have been performed using the Vienna *ab initio* simulation package (VASP),[49,50] which was recently extended to deal with fully unconstrained noncollinear magnetic structures,[51] and which was extended further in the context of this work to exploit the translational symmetry of helical spin structures in terms of the application of generalized Bloch conditions to the Hamiltonian.[52,53] To describe the electron-ion interactions, VASP employs the full-potential all-electron projector-augmented-wave (PAW) method introduced by Blöchl.[54,55] VASP makes no shape approximation to the charge and magnetization density, nor to the electronic potential, and therefore allows not only for interatomic but also for intra-atomic noncollinearity of the magnetization. Accounting for the intra-atomic noncollinearity of the magnetization density and the use of the full electronic potential, without shape approximations, were already shown to be crucial when dealing with spin spirals in γ-Fe.[47] For our calculations of the spin-spiral states we used the gradient-corrected exchange-correlation functional of Perdew, Burke, and Ernzerhof,[56] and the spin-interpolation proposed by Vosko, Wilk, and Nusair.[57] The calculations of collinear magnetic structures of Spišák *et al.*,[35,37,38] which we will shortly discuss later on, were performed using the exchange-correlation functional of Perdew and Zunger[58] and the generalized-gradient approximation of Perdew *et al.*[59] We do not expect, however, that this difference in exchange-correlation potentials will taint a comparison between our calculations and the aforementioned studies of Spišák *et al.*

The use of gradient-corrected exchange-correlation functionals in connection with noncollinear magnetism deserves a few remarks. The gradient-corrected functionals depend on n, $|\vec{m}|$, ∇n, and $\nabla|\vec{m}|$, i.e., the electronic density, the magnetization density, and their respective gradients. As such, strictly speaking, these functionals do not apply to the case of noncollinear magnetism since they do not incorporate any dependence on changes in the direction of the magnetization. We proceed by projecting the gradient of the magnetization in every point in space onto the direction of the magnetization at these points. This projected quantity, which can be seen as the gradient with respect to a "local" spin quantization axis (an axis which can be different for every point in space), is then used in the gradient-corrected functionals. That we may use gradient-corrected functionals despite the previous considerations is justified by the observation that on the intra-atomic scale the magnetization density tends to be largely collinear (the direction of the magnetization varies only slowly).

In all our calculations, the integrations over the first Brillouin zone were done on a $13 \times 13 \times 13$ Monkhorst-Pack[60] grid of k points, using the tetrahedron method with the corrections proposed by Blöchl.[61] Our study of the stability of helical magnetic configurations with propagation vectors along Γ-X and X-W, against tetragonal and orthorhombic

TABLE I. Equilibrium atomic volume Ω, axial ratio c/a, magnetic moment m, and energy difference ΔE for fct-Fe, in the ferromagnetic (FM), bilayer antiferromagnetic (biAFM), and single layer antiferromagnetic state (AFM), as taken from Ref. 35.

	Ω (Å^3)	c/a	m (μ_B)	ΔE (meV)
FM	11.59	1.18	2.35	20.5
biAFM	11.00	1.10	2.06	0.0
AFM	10.42	1.06	1.52	5.2

distortions of the fcc structure were done using a primitive cell defined by the lattice vectors $a\times(0,b/2a,c/2a)$, $a\times(1/2,0,c/2a)$, and $a\times(1/2,b/2a,0)$. The monoclinic shearing of the fct structure reported by Spišák et $al.$[37,38] was modeled using a base-centered monoclinic primitive cell spanned by the vectors

$$\frac{a}{\sqrt{2}}\times\left(\frac{\sqrt{2}}{2}\frac{c}{a},\frac{1}{2},\frac{1-\delta}{2}\right), \qquad \frac{a}{\sqrt{2}}\times\left(\frac{\sqrt{2}}{2}\frac{c}{a},-\frac{1}{2},\frac{1-\delta}{2}\right),$$

and

$$\frac{a}{\sqrt{2}}\times(0,0,1),$$

where one obtains the fcc structure for $c/a=1$ and $\delta=0$. For $\delta\neq0$ this cell describes the shearing of $\{111\}$ planes along $\langle110\rangle$ directions.

III. SHEAR INSTABILITY OF FCC FE IN COLLINEAR MAGNETIC CONFIGURATIONS

Before we present our results for the helical spin solutions, it is appropriate to discuss the structural optimization of bulk γ-Fe for several collinear magnetic configurations. Spišák et $al.$ optimized the crystalline structure of γ-Fe in the ferromagnetic (FM), single layer antiferromagnetic (AFM), and bilayer antiferromagnetic (biAFM) states, and found that in all three magnetic configurations bulk γ-Fe is unstable against tetragonal distortion.[35] In the FM and biAFM magnetic state the structure is in addition to the tetragonal distortion also unstable against both tetragonal as well as monoclinic shearing deformations of the fcc lattice.[37,38] Tables I and II summarize their findings for the equilibrium structure of γ-Fe in the FM, AFM, and biAFM magnetic configuration.

In the fct phase the biAFM configuration is found to be lower in energy than both the FM and AFM states. The amount of tetragonal distortion increases with the ferromagnetic component of the magnetic coupling. For both the FM and biAFM configurations the fct structure represents only a saddle point on the potential energy surface $E(c/a,\delta)$, i.e., monoclinic shearing lowers the total energy. The shear distortion increases in proportion to the ferromagnetic component. It is remarkable that the calculated shearing angle $\varphi=\arctan\delta$ of 18.4° comes very close to the angle measured in the STM studies on ultrathin Fe/Cu(001) films.[27]

TABLE II. Axial ratio c/a, monoclinic shearing deformation δ, magnetic moment m, and energy difference ΔE for monoclinically sheared fct-Fe, in the ferromagnetic (FM), bilayer antiferromagnetic (biAFM), and single layer antiferromagnetic state (AFM), as taken from Ref. 38. The axial ratio and monoclinic deformation were optimized at a series of fixed lattice constants. Shown here are the results for $a_0=3.40$ Å^3, the equilibrium lattice constant for FM fct-Fe (upper three entries), and for $a_0=3.64$ Å^3, the theoretical lattice parameter of bulk Cu (lower three entries). ΔE is given with respect to the energy of the equilibrium structure of fct-Fe in the biAFM state (see Table I).

Ω (Å^3)	Config.	c/a	δ	m (μ_B)	ΔE (meV)
11.50	FM	1.17	0.33	2.23	-129.1
11.20	biAFM	1.14	0.17	2.06	-70.9
10.71	AFM	1.09	0.00	1.55	-49.2
12.18	FM	1.01	0.26	2.44	-53.2
11.94	biAFM	0.99	0.13	2.23	-8.1
11.70	AFM	0.97	0.00	1.79	49.6

IV. SPIRAL SPIN-WAVES IN FCC FE

Tsunoda et $al.$[15] characterized the ground state of the γ-A phase (coherent fcc) of Fe precipitates in Cu to be a spin-spiral state propagating with wave vector $\vec{q}_{exp}=2\pi/a\times(0.1,0,1)$. Recently Knöpfle et $al.$[47] were able to reproduce these findings in the framework of DFT calculations when they found a wave vector of $\vec{q}=2\pi/a\times(0.15,0,1)$ for the spin-spiral ground state of γ-Fe, at volumes up to 11.37 Å^3 (slightly below the experimentally determined volume of 11.44 Å^3). As mentioned before, however, ASW methods tend to overestimate the equilibrium volume, and the question whether DFT in principle yields the correct spin-spiral ground state at the equilibrium volume remains therefore unanswered. Considering the fact that the equilibrium volumes of the ferromagnetic low- and high-moment (FM-LM and FM-HM) states and the single layer antiferromagnetic (AFM) state of (undistorted) γ-Fe as calculated by Spišák et $al.$[35] using the PAW method, are considerably lower than the equilibrium volumes determined by Knöpfle et $al.$ for these magnetic configurations (FM-LM: 10.49 Å^3 vs 12.00 Å^3, FM-HM: 12.26 Å^3 vs 12.74 Å^3, and AFM: 10.63 Å^3 vs 11.11 Å^3), it is probable that DFT in general will not stabilize the correct spin-spiral up to the volume found by the latter authors. (The PAW results of Ref. 35, incidentally, are in good agreement with the FLAPW calculations of Herper et $al.$[46]) We calculated the spin-spiral dispersion along Γ-X and X-W at a number of different volumes ranging from 10.45 to 11.69 Å^3, and in agreement with previous theoretical studies we find at all volumes two (local) minima: at $\vec{q}_1=2\pi/a\times(0,0,0.6)$ between Γ and X, and at $\vec{q}_2=2\pi/a\times(0.2,0,1)$ between X and W, where the latter more or less corresponds to $\vec{q}_{exp}$. Figure 1 shows the spin-spiral dispersion along Γ-X and X-W at a few different volumes, as calculated in the present work [note that the volume of 11.44 Å^3 corresponds to the equilibrium volume of the A
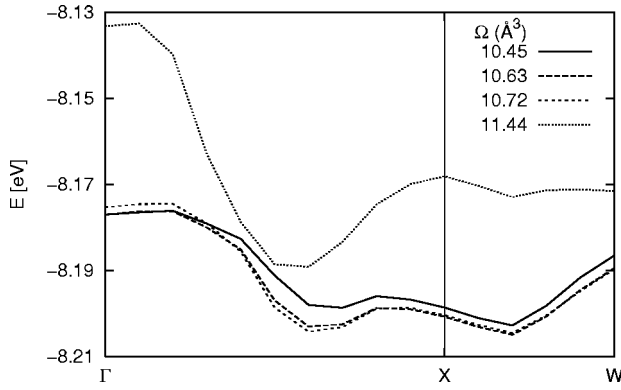
FIG. 1. Volume dependence of the spin-spiral dispersion along Γ-X and X-W, in fcc-Fe (γ-Fe). At low volumes, up to $\Omega = 10.63$ Å^3, the magnetic configuration corresponding to the groundstate is a spin-spiral at $\vec{q}_2 = \frac{2}{5}XW$, whereas for higher volumes the helical spin configuration at $\vec{q}_1 = \frac{6}{10}\Gamma X$ is lowest in energy. Note that at the experimental volume of γ-Fe precipitates in Cu ($\Omega = 11.44$ Å^3), the ground-state magnetic configuration is found to be the spin-spiral $\vec{q}_1$, in disagreement with the spin-spiral ground state at $\vec{q}_{exp} = \frac{1}{5}XW$, as found in experiment.

phase of γ-Fe precipitates in Cu as determined by Tsunoda *et al.* (see, for instance, Ref. 12)].

As suspected, we indeed find that the experimentally determined spiral wave vector corresponds to the ground state only at considerably lower volume than was reported in the study by Knöpfle *et al.*, up to a volume of 10.63 Å^3 instead of 11.37 Å^3. According to our calculations the spiral solution $\vec{q}_2$ at a volume of 10.63 Å^3 constitutes the global minimum. It is, however, nearly degenerate with the helical spin solution with propagation vector $\vec{q}_1$ at a volume of 10.81 Å^3 (see Fig. 2). The latter spiral solution characterizes the magnetic configuration of the groundstate at volumes above 10.72 Å^3.

To determine the most stable helical spin configuration one should, in principle, sample the complete irreducible wedge of the Brillouin zone, instead of the limited search along Γ-X and X-W presented here. This would be computationally far too demanding. We have therefore limited ourselves to confirming that the solutions at $\vec{q}_1$ and $\vec{q}_2$ correspond to true (local) minima and not to saddle points, by establishing that taking the propagating vector away from $\vec{q}_1$ and $\vec{q}_2$ along directions perpendicular to, respectively, Γ-X and X-W, raises the total energy of the spin spiral.

In addition to the $\vec{q}_1$ and $\vec{q}_2$ spiral states, Fig. 2 also shows the volume dependence of our spiral solutions at Γ and X. The spin-spiral solutions at Γ and X correspond to, respectively, FM and AFM states, and can be compared—to validate our implementation of the spiral symmetry—to the collinear magnetic configurations studied by Spišák *et al.* (see Table I). The equilibrium volumes of 10.54, 12.10, and 10.63 Å^3, for the low- and high-moment states at Γ ($m_{LM} \approx 1.00\mu_B$; $m_{HM} = 2.60\mu_B$), and the spin-spiral state at X ($m = 1.36\mu_B$), respectively, are in good agreement with the collinear calculations of Refs. 35 and 46.
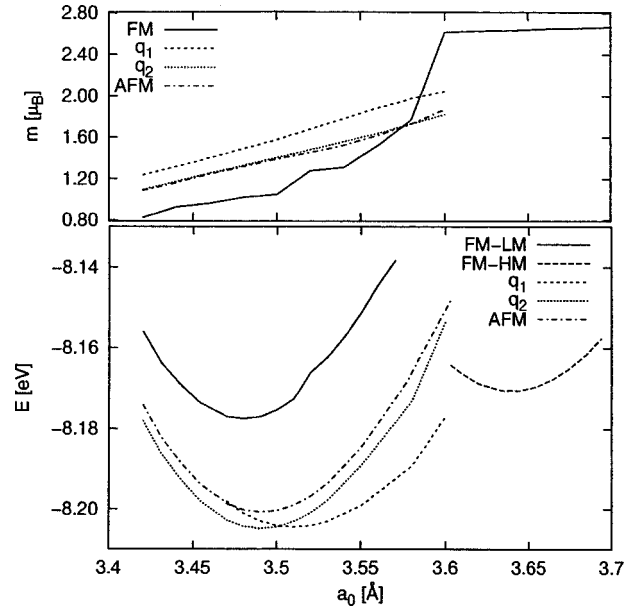
That an helical spin configuration at X can be taken to

FIG. 2. Total energy E and magnetization m, versus volume, for several important magnetic configuration in fcc-Fe (γ-Fe). Shown here are the low- and high-moment ferromagnetic states, FM-LM and FM-HM, the single layer antiferromagnetic state (AFM), and the helical spin configurations, $\vec{q}_1 = \frac{6}{10}\Gamma X$ and $\vec{q}_2 = \frac{2}{5}XW$, corresponding to the two (local) minima in the spin-spiral dispersion along Γ-X-W (see also Fig. 1). Note especially the (near) degeneracy of the spin-spiral solutions $\vec{q}_1$ and $\vec{q}_2$ at their respective equilibrium volumes of 10.63 and 10.81 Å^3 (i.e., $a_0 = 3.49$ and 3.51 Å).

correspond to a collinear calculation of the AFM state is not a trivial statement. It is in fact only true because the magnetization tends to be largely collinear on the intra-atomic scale. The noncollinearity of the magnetization of a spin-spiral exhibits itself in the interatomic domains where the magnitude of the magnetizations is very small. The above is exemplified in Fig. 3 for a spin-spiral with propagation vector $\vec{q}_1$. Close to the nucleus, where the magnetization density is large, the magnetization is almost exactly collinear. In the interstitial regions, rotations over 180° occur over very small distances—but in these regions the magnetization is close to zero. This result underlines that the intraatomic noncollinearity is weak but a full-potential treatment is crucial to stabilize the spin spiral with the correct propagation vector.

V. SPIRAL SPIN-WAVES AT BROKEN CUBIC SYMMETRY

A. Face-centered tetragonal Fe

To our knowledge the only previous attempt at describing the effects of a lowering of the cubic symmetry on the stability of the spin-spiral solutions in γ-Fe can be found in a study by Körling and Ergon,[62] who calculated the dispersion along Γ-X-W-Γ for $c/a = 0.95$ and 1.05, at a lattice constant of 3.61 Å, using the LMTO-ASA method. These authors, however, failed to produce a (local) minimum between X and W, and their calculations hardly constitute a comprehensive search through the ($\Omega, c/a, \vec{q}$) parameter space. We have calculated the spin-spiral dispersion of tetragonally distorted
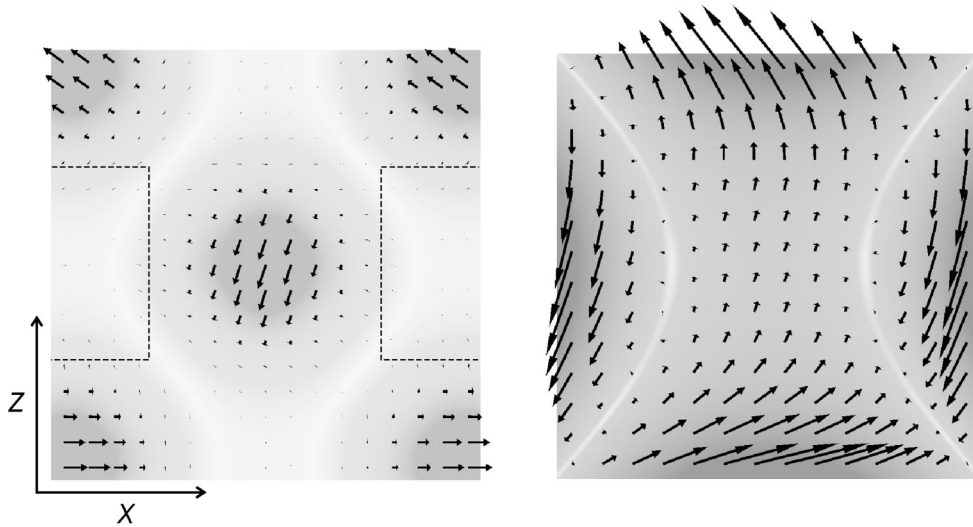
FIG. 3. The magnetization field of a spin-spiral with propagation vector $\vec{q}_1$ (along the z direction), on a $a_0 \times a_0$ xz plane centered on an atomic position (upper figure), and magnified on a $\frac{1}{2}a_0 \times \frac{1}{2}a_0$ xz plane centered between the atomic positions (lower figure). (The length of the vectors and the shading of the planes correspond to the magnitude of the magnetization, n.b., the shading in the two figures is not equivalent.)

(fct) γ-Fe along Γ-Z and Z-U, where $U = 2\pi/a \times (1/2,0,a/c)$ (see Fig. 4), for $0.92 \leq c/a \leq 1.12$, at a series of different volumes ranging from 10.45 to 11.69 Å^3. Figure 5 shows the spin-spiral dispersion along Γ-Z and Z-U for $c/a = $ 1.02, 1.04, 1.08, and 1.12, at different volumes. To describe the influence of tetragonal distortions on the spiral dispersion it is convenient to differentiate between two volume ranges $\Omega < 11.00$ Å^3 and $\Omega > 11.00$ Å^3.

Below a volume of approximately 11.00 Å^3 tetragonal distortions with $c/a > 1$ tend to raise the energy of solutions around Γ (up to $\frac{1}{3}\Gamma Z$) and generally lower the total energy of the spiral dispersion in the neighborhood of Z (roughly all solutions between $\frac{1}{3}\Gamma Z$-Z-$\frac{1}{3}ZU$). Moderate tetragonal distortions, with $c/a \leq 1.04$ stabilize the helical spin configuration at $\vec{q}_2$ over the solution at $\vec{q}_1$, i.e., the range at which $\vec{q}_2$ corresponds to the ground state of the system is extended to larger volumes [up to $\Omega = 10.99$ Å^3 for $c/a = 1.04$; with $\vec{q}_2 = 2\pi/a \times (0.1,0,a/c)$]. Larger tetragonal distortions however shift $\vec{q}_2$ towards Z, at $c/a \geq 1.08$, the minimum along Z-U has disappeared, and the ground state of the system is located at Z.

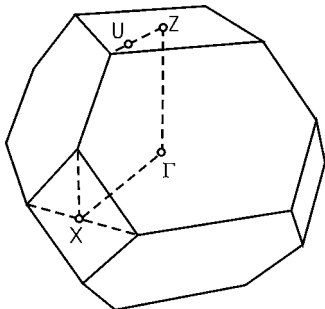At volumes above 11.00 the situation is quite different. Tetragonal distortions with $1 < c/a \leq 1.12$ lower the total energy of the spiral dispersion along almost the complete path through the Brillouin zone we investigated, from Γ-Z and from Z up to approximately $\frac{1}{2}ZU$. In contrast to the results for $\Omega < 11.00$ Å^3 the effects are strongest around Γ, and tetragonal distortions stabilize the minimum at $\vec{q}_1$ even further over the solution at $\vec{q}_2$. Actually for $c/a \geq 1.04$ the minimum along Z-U has already disappeared completely. At $\Omega > 11.00$ Å^3 the total energy of fct-Fe is minimized for a spin spiral with propagation vector $\vec{q}_1$, at a volume of 11.18 Å^3, with $c/a \approx 1.10$. The global minimum, however, is located at Z, for a tetragonal distortion of $c/a = 1.08$, at a volume of 10.81 Å^3.

Table III lists the optimized fct structural parameters for the (local) minima at Γ, $\vec{q}_1$, Z, and $\vec{q}_2$ (see also Fig. 6). The spin-spiral dispersion relations along Γ-Z-U for these fct structures are depicted in Fig. 7. Actually, $\vec{q}_2$ is not a true local minimum in the $(\Omega, c/a, \vec{q})$ parameter space of the fct structure, since it is unstable against small changes in volume and c/a ratio, and there is no energy barrier between the points $(10.63, 1.06, \vec{q}_2)$ and $(10.81, 1.08, Z)$. ("$\vec{q}_2$," however, obviously does represent a minimum with respect to changes in the propagation vector, and as such it was added to Table III and Fig. 7.) As in the previous section, the equilibrium structures at Γ and Z may be compared to the collinear FM and AFM configurations studied by Spišák *et al.* We find our values for Ω and c/a at Γ and Z to be in reasonable agreement with the results listed in Table I. It is tempting to compare the helical spin configuration at $\vec{q}_1$ (or at $\frac{1}{2}\Gamma Z$) to the biAFM ($\uparrow\uparrow\downarrow\downarrow$) structure (see Table I), and the fact that the equilibrium volume and c/a ratio for these magnetic configurations agree quite closely would encourage one to do so.
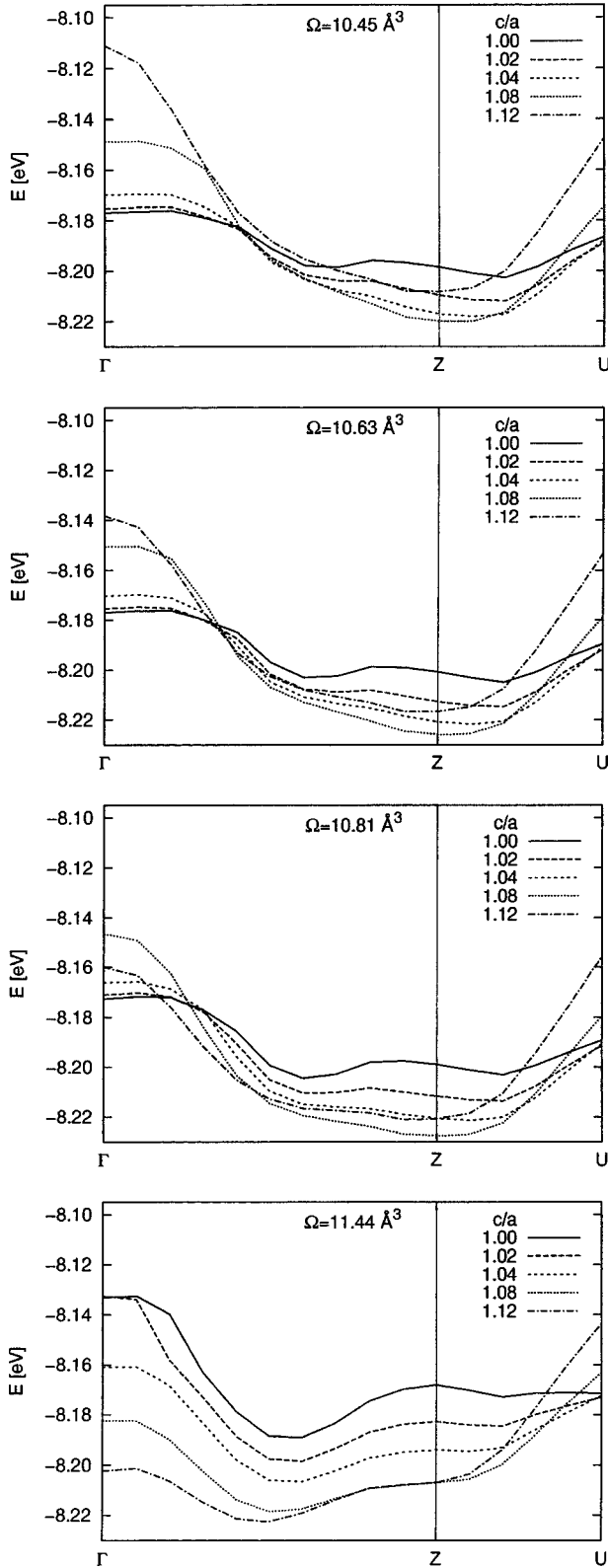

FIG. 4. Brillouin zone of the fct structure.

FIG. 5. Spin-spiral dispersion in fct-Fe, for $\Omega = 10.45$, 10.63, 10.81, and 11.44 Å^3.

These magnetic configurations, however, are quite distinct from each other and calculations employing the spiral symmetry to a unit cell containing a single atom cannot produce *collinear* spin-density waves. Spišák *et al.* have shown the

TABLE III. Optimized structural parameters (atomic volume Ω and axial ratio c/a), magnetic moment m, and energy differences ΔE, for fct-Fe at fixed magnetic configuration $\vec{q}$ (corresponding collinear magnetic configurations are stated between brackets). Note that the entries for "Γ," $\vec{q}_1$, and Z, represent true (local) minima in the (Ω, c/a, $\vec{q}$) parameter space, whereas the other configurations are stable against changes in Ω and c/a only at fixed $\vec{q}$.

$\vec{q}$	Ω (Å^3)	c/a	$m(\mu_B)$	ΔE (meV)
Γ (FM)	11.69	1.18	2.37	10.3
$\frac{1}{2}\Gamma Z$	11.18	1.12	2.10	4.2
$\vec{q}_1$	11.18	1.10	2.01	3.4
Z (AFM)	10.81	1.08	1.62	0
$\vec{q}_2$	10.63	1.06	1.50	2.1

biAFM configuration, i.e., a collinear spin-density wave at $\frac{1}{2}\Gamma Z$, to correspond to the ground state in fct-Fe. The biAFM structure is favored over the AFM structure by about 5 meV, whereas the helical spin configuration at $\vec{q}_1$ is 3.4 meV *higher* in energy than the spin spiral at Z (which to a certain degree corresponds to the AFM structure).

As in the previous section one can again justly argue that the sampling of $\vec{q}$ space is very limited when only considering helical spiral configurations with propagation vectors along Γ-Z and Z-U. This situation is even compounded due to the lowering of the symmetry, since for the fct structure
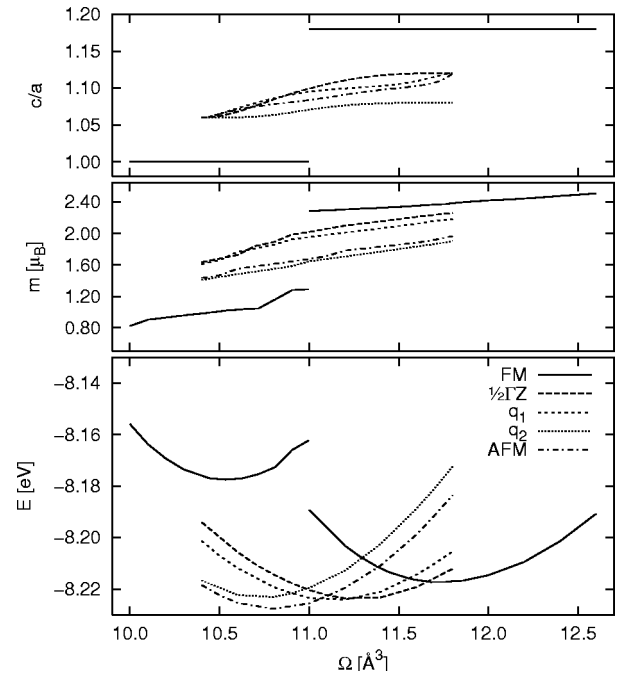

FIG. 6. Energy E, magnetic moment m, and axial ratio c/a versus atomic volume Ω, for fct-Fe in the FM state, the single layer AFM state, and for the helical spin configurations with propagation vectors $\vec{q} = \frac{1}{2}\Gamma Z$, $\vec{q}_1$, and $\vec{q}_2$. In the FM state, a discontinuous transition from a cubic low-moment to a tetragonal high-moment state occurs at $\Omega \approx 11.0$ Å^3.
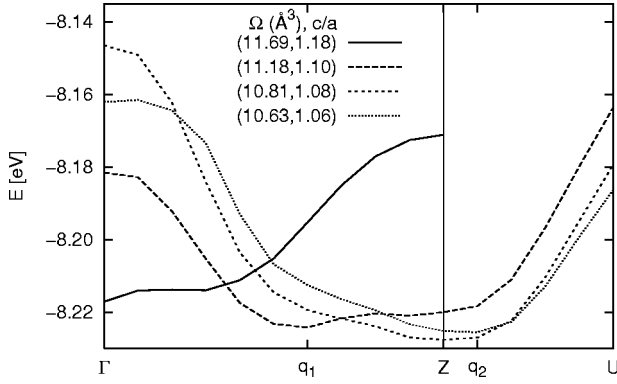
FIG. 7. Spin-spiral dispersion along Γ-X-W for the fct structures with $(\Omega, c/a) = (11.68, 1.18)$ dispersion along X-W not calculated, $(11.18, 1.10)$, $(10.81, 1.08)$, and $(10.63, 1.06)$ [all volumes in Å³]. The first three curves show the (local) minima in the fct-Fe $(\Omega, c/a, \vec{q})$ parameter space, at $\vec{q} = \Gamma$ (FM), $\vec{q}_1$, and Z (AFM), respectively (see also Table III).

the path from Γ to Z is no longer equivalent to Γ-X (as was the case in the cubic structure). The choice to limit our study almost completely to spiral configurations along Γ-Z (and the related Z-U direction) and to all but neglect to consider spin-spirals propagating in the Γ-X direction can to a certain degree be justified from symmetry arguments, because along Γ-Z the crystalline and magnetic structure break the cubic symmetry along the same axis. We have calculated the influence of tetragonal distortions on the spin-spiral dispersion along Γ-X for a very limited number of volumes ($\Omega = 10.63$, 10.81, and 11.44 Å³). As is exemplified in Fig. 8, γ-Fe is stable against tetragonal distortions for helical spin configurations with $\vec{q} > \frac{1}{3}\Gamma X$ along Γ-X. The effects of tetragonal distortions on the spin-spiral dispersion between Γ and $\frac{1}{3}\Gamma X$ are similar to those described for the dispersion between Γ and $\frac{1}{3}\Gamma Z$, where for volumes below 11.00 Å³ the system is stable against tetragonal distortions as opposed to the situation at volumes above 11.00 Å³ where large tetragonal distortions are favored for these near FM states (see Fig. 5).
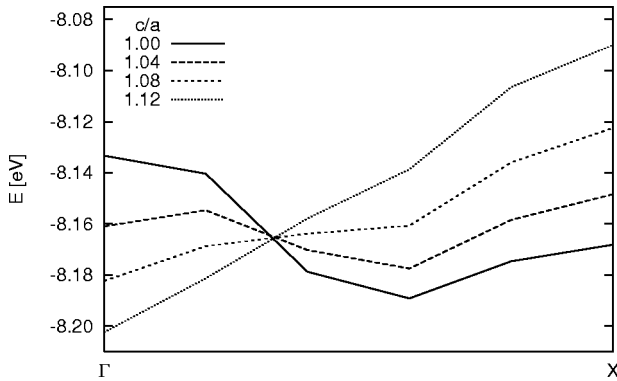

FIG. 8. Spin-spiral dispersion along Γ-X (perpendicular to the tetragonal axis) in fct-Fe, for $\Omega = 11.44$ Å³, and varying axial ratio c/a.
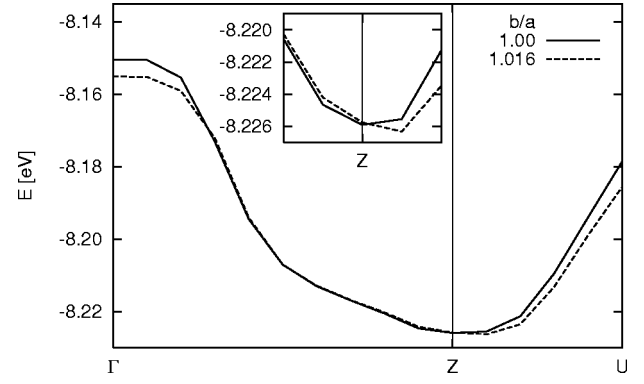

FIG. 9. The influence orthorhombic distortions ($b/a \neq 1$) of the fct structure on the spin-spiral dispersion, for $\Omega = 10.63$ Å³ with $c/a = 1.08$.

B. Orthorhombic distortions

The helical spin solutions away from Z along Z-U not only break the cubic symmetry, but depart from tetragonal symmetry as well. Considering the symmetry of the magnetic configurations along Z-U it therefore makes sense to check the stability of fct-Fe against orthorhombic distortions. Since this adds yet another parameter to a computationally already overtaxing optimization problem we have limited ourselves to optimizing the c/a and b/a ratio's for the spin-spiral configurations near $\vec{q}_2$ at volumes below 11.00 Å³. One should note here that in our calculations $b/a > 1$ denotes an elongation of the cubic cell in the same direction Z-U along which we previously found the spiral solution $\vec{q}_2$. (This is nontrivial since an orthorhombic distortion breaks the C_4 symmetry, and the path Z-U through the Brillouin zone is no longer fourfold degenerate.) Small orthorhombic distortions ($b/a \approx 1.02$) of the fct structure do tend to lower the energy of spin-spiral solutions away from Z along Z-U with respect to the solution at Z, over the whole volume range we considered. Figure 9 shows how an orthorhombic distortion of $b/a = 1.016$ of the fct structure with $c/a = 1.08$ at a volume of 10.63 Å³ shifts the global minimum from Z to $\vec{q}_2$. The energy difference involved, however, is so small that one may easily consider these states to be degenerate (see inset in Fig. 9). Furthermore, although orthorhombic distortions marginally stabilize a spin-spiral solution at $\vec{q}_2$ over the solution at Z for the undistorted fct structure for volumes up to 10.72 Å³, the optimal structure of fct-Fe, i.e., $c/a = 1.08$ at a volume of 10.81 Å³ with $\vec{q} = Z$ (see Table III) is actually stable against orthorhombic distortions (albeit again almost degenerate with the solution at $\vec{q}_2$ for $b/a = 1.016$).

C. Monoclinic shear deformation

We have studied the stability against monoclinic shearing for three of the fct structures listed in Table III: (i) $\Omega = 11.69$ Å³ with $c/a = 1.18$, (ii) $\Omega = 11.18$ Å³ with $c/a = 1.10$, and (iii) $\Omega = 10.81$ Å³ with $c/a = 1.08$, (see Fig. 7), i.e., the FM, SS-$\vec{q}_1$, and AFM, (local) minima in the fct parameter space. Since, as before, it is intractable to perform
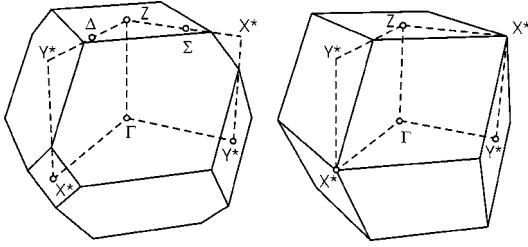
FIG. 10. Brillouin zone of the sheared fct structure, for c/a $= 1.18$ with $\delta = 0.15$ (left), and $\delta = 0.35$ (right).

a rigorous sampling of the BZ in $\vec{q}$ space, we have again calculated the spin-spiral dispersion only along a limited number of special lines through the BZ. The problem of selecting a path through the BZ, appropriate for comparison with the fct structure, is compounded by the fact that the BZ changes shape, and the only special points that the BZ of the fct structure and the monoclinically sheared fct structure have in common are Γ and Z. We chose to investigate the effects of monoclinic shearing on the spin-spiral dispersion along Γ-Z, Γ-X^*, and Γ-Y^* for fct structure (i), along Γ-Z for structure (ii), and along Γ-Z, Z-Δ, and Z-Σ for structure (iii). The points Δ, Σ, X^*, and Y^* correspond to $2\pi/a$ $\times(\frac{1}{2}+\delta/2\sqrt{2}, -\delta/2\sqrt{2}, a/c)$, $2\pi/a\times(\delta/2\sqrt{2}, \frac{1}{2}-\delta/2\sqrt{2}, a/c)$, $2\pi/a\times(1+\delta/\sqrt{2}, -\delta/\sqrt{2}, 0)$, and $2\pi/a\times(\delta/\sqrt{2}, 1-\delta/\sqrt{2}, 0)$, respectively, where for $\delta=0$, Δ and Σ reduce to U, and X^* and Y^* are equivalent to X (see Fig. 10 and compare with Fig. 4).

The results compiled in Fig. 11 demonstrate that in the geometry optimized in the FM configuration, fct-Fe is unstable against monoclinic shear deformations. For spin-spirals with propagation vectors oriented along Γ-X^*, a shear distortion of $\delta \sim 0.30$ leads to the lowest energy at all wavevectors. For propagation vectors along Γ-Y^* and Γ-Z, monoclinic shearing lowers the energy only up to halfway from the center to the boundary of the BZ, which demonstrates again that shearing is favored by a ferromagnetic component of the polarization. Around the atomic volume and geometry favoring the commensurate AFM state (iii), the instability of fct-Fe against monoclinic shearing persists from $\vec{q}=\Gamma$ up to approximately $\frac{1}{2}\Gamma Z$ (see the lower panel of Fig. 12). However, it is important to emphasize that for structure (iii) the minimum at Γ for $\delta=0.35$ is only a few meV lower than that of the commensurate AFM (Z) state in the tetragonal ($\delta=0$) geometry. Upwards from $\frac{1}{2}\Gamma Z$ along Γ-Z structure (iii) is stable against monoclinic shearing. The results of our calculations on the effects of shearing on the spin-spiral dispersion along Γ-Z for fct structure (ii) are not shown here, because they are qualitatively identical to the results of our calculations on structure (i).

Our limited survey of the $(\Omega, c/a, \delta, \vec{q})$ parameter space places the equilibrium structure of monoclinically sheared fct-Fe at $\Omega = 11.69$ Å^3, $c/a = 1.18$, $\delta = 0.35$, and $\vec{q}=\Gamma$ (FM), which is in good agreement with the calculations of Spišák et al.,[38] who performed a more thorough optimization of Ω, c/a, and δ for the ferromagnetic state (see Table II). The observation that an instability against monoclinic shear-
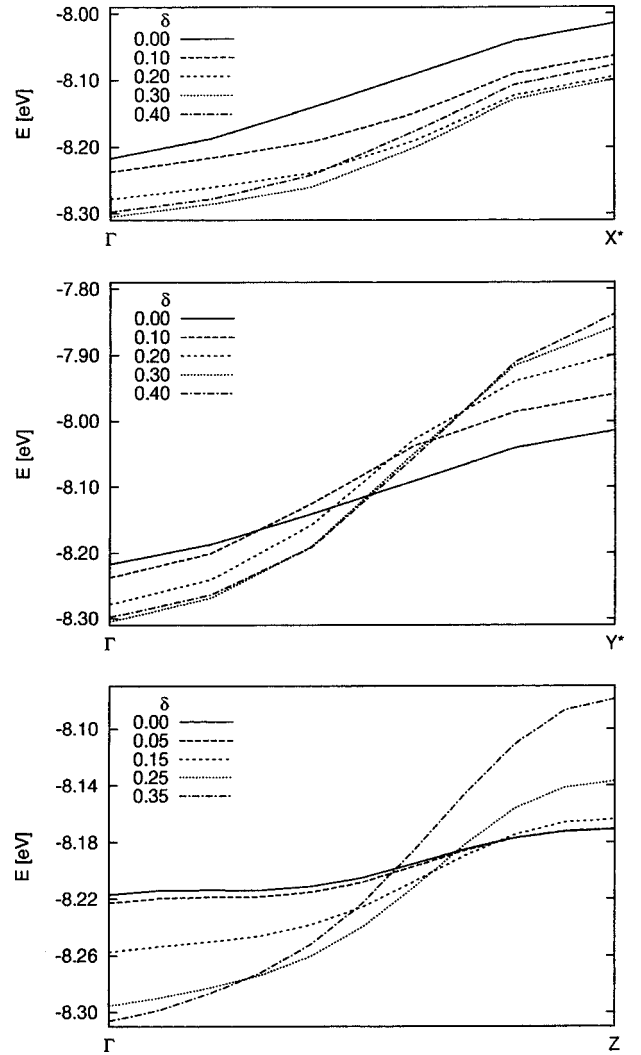

FIG. 11. Spin-spiral dispersion along different symmetry lines in monoclinically sheared fct-Fe, for $\Omega = 11.69$ Å^3, with $c/a = 1.18$

ing appears only in combination with a appreciable ferromagnetic component in the magnetic configuration is also consistent with the results of results of Spišák et al., who showed the bilayer AFM state to be unstable, and the single layer AFM state to be stable against monoclinic shearing of the fct structure (see Table II).

The lowering of the symmetry ($C_{4h} \rightarrow C_{2h}$) due to the shearing distortion, and the resulting inequivalence of the Γ-X^* and Γ-Y^* paths through the BZ, are clearly visible in the two upper panels of Fig. 11. The stability/instability of the fct-structure against monoclinic shearing for helical spin configurations propagating along Γ-Y^* is (qualitatively) very similar to the effects of the shearing distortion on the spin-spiral dispersion along Γ-Z; magnetic configurations with $\Gamma < \vec{q} < \frac{1}{2}\Gamma Y^*$ stabilize the fct structure, whereas for $\frac{1}{2}\Gamma Y^* < \vec{q} < Y^*$ the fct structure shows a tendency to shear. For magnetic configurations with $\vec{q} \in \Gamma$-X^*, however, the fct structure is unstable against monoclinic shearing along the complete path through the BZ. Similarly, the influence of the
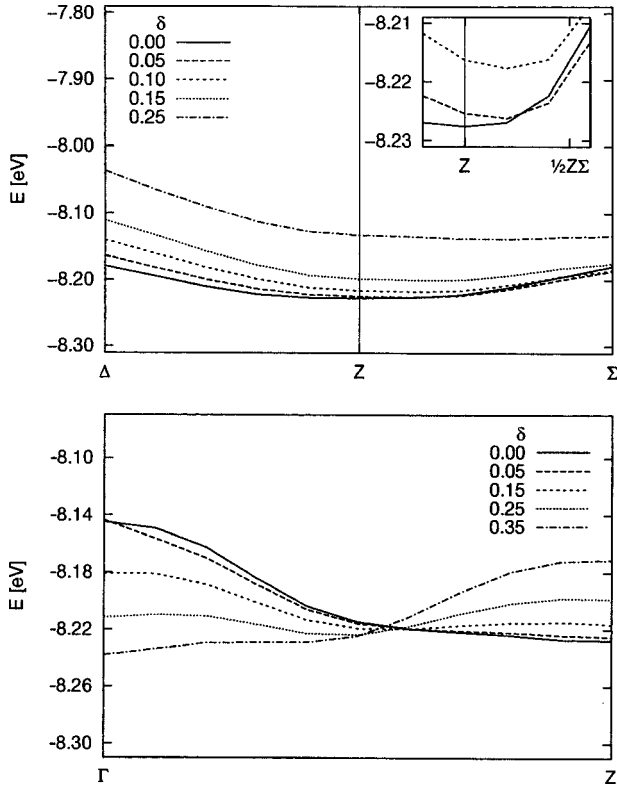
FIG. 12. Spin-spiral dispersion along different symmetry lines in monoclinically sheared fct-Fe, for $\Omega = 10.81$ Å^3, with $c/a = 1.08$

TABLE IV. Summary of the optimization of the crystalline and magnetic structure for fcc, fct, and monoclinically sheared fct Fe. Listed are the structural parameters, i.e., atomic volume Ω, axial ratio c/a, and monoclinic shearing deformation δ, and the propagation vector $\vec{q}$ of the magnetic configuration corresponding to the ground state in these structures.

	$\vec{q}$	Ω (Å^3)	c/a	δ	ΔE (meV)
fcc	$\vec{q}_2$	10.63	1.00	0.00	101.7
	$\vec{q}_1$	10.81	1.00	0.00	101.3
fct	Z	10.81	1.08	0.00	78.0
sheared	Γ	11.69	1.18	0.35	0.0

ration with propagation vector $\vec{q}_2 = 2\pi/a \times (0.2,0,1)$. Going to higher volumes we find, at 10.72 Å^3, a transition in the magnetic ordering, from the spin-spiral state $\vec{q}_2$ into another helical configuration with propagation vector $\vec{q}_1 = 2\pi/a \times (0,0,0.6)$. At even higher volumes, $\Omega > 11.76$ Å^3 ($a_0 = 3.61$ Å), the system undergoes a second transition and orders ferromagnetically. The global minimum is found at a volume of 10.63 Å^3 for a spin-spiral solution with propagation vector $\vec{q}_2$, which corresponds quite favorably with the experimentally determined propagation vector $\vec{q}_{\exp} = 2\pi/a \times (0.1,0,1)$. This solution, however, is almost degenerate in total energy with the spin-spiral state $\vec{q}_1$ at a volume of 10.81 Å^3 (see Table IV). (The spin-spiral dispersion between $\vec{q}_1$ and $\vec{q}_2$ along Γ-X-W at these volumes is in fact so flat—the spread is around 5 meV—that one could consider all states between $\vec{q}_1$ and $\vec{q}_2$ to be degenerate.) Furthermore, at the volume of γ-Fe precipitates in Cu, $\Omega = 11.44$ Å^3 ($a_0 = 3.577$ Å, see, for instance, Ref. 12), our calculations predict the spin-spiral solution at $\vec{q}_1$ to correspond to the groundstate, in obvious disagreement with experiment.

Our results, on the other hand, are in excellent agreement with previous theoretical studies of collinear magnetic configuration in γ-Fe,[35,46] which is an important observation since it establishes the validity of our implementation of the spiral symmetry.

fct-Fe. We have calculated the spin-spiral dispersion of tetragonally distorted (fct) γ-Fe along Γ-Z and Z-U (see Fig. 4), for $0.92 \leq c/a \leq 1.12$, at a series of different volumes ranging from 10.45 to 11.69 Å^3. At volumes above approximately 11.00 Å^3 tetragonal distortions lower the energy of spin-spiral solutions along Γ-Z (more so around Γ than around Z) and stabilize the spin-spiral solution $\vec{q}_1$ over the solution at $\vec{q}_2$ even stronger than already was the case for fcc-Fe. For $\Omega < 11.00$ Å^3 tetragonal distortions raise the energy of spiral solutions in the neighborhood of Γ and lower them around Z. In the latter volume range, moderate tetragonal distortions tend to stabilize the spiral solution $\vec{q}_2$ over the solution at $\vec{q}_1$. However with increasing c/a the minimum along Z-U shift towards Z and for $c/a \geq 1.08$ the system orders antiferromagnetically. Our calculations yield three (local) minima in the $(\Omega, c/a, \vec{q})$ parameter space of the

shearing distortion on the spin-spiral dispersion along the paths Z-Δ and Z-Σ also differ from each other. For helical magnetic configuration propagating along Z-Δ, the fct structure is stable against monoclinic shearing. A continuation along this direction beyond Σ ends up in Y^* where the same stability was found for structure (i) (see Figs. 10 and 11). Along Z-Σ, the behavior is different and as can be seen in the inset of the upper panel of Fig. 12, monoclinic shearing of structure (iii) produces a local minimum at approximately $\frac{1}{5}Z\Sigma$ (analogous to $\vec{q}_2$ along X-W or Z-U).

VI. DISCUSSION

We have studied the influence of structural distortions on the spin-spiral magnetism in γ-Fe. To this end we calculated the spin-spiral dispersion in fcc-Fe (γ-Fe), fct-Fe, orthorhombically distorted fct-Fe, and monoclinically sheared fct-Fe, along several directions of "high" symmetry in their respective Brillouin zones. The results may be summarized as follows.

fcc-Fe. We calculated the spin-spiral dispersion along Γ-X and X-W in γ-Fe at a number of different volumes ranging from 10.0 to 12.7 Å^3. As is shown in Fig. 2, and as was already clear from previous theoretical studies, the magnetic configuration of the ground state in γ-Fe strongly depends on the assumed atomic volume. At volumes between 10.00 and 10.72 Å^3 ($3.42 < a_0 < 3.5$ Å) the magnetic configuration corresponding to the ground state is a helical spin configu-

fct structure, $(11.69, 1.18, \Gamma)$, $(11.18, 1.10, \vec{q}_1)$, and $(10.81, 1.08, Z)$. The total energy is minimized by the solution at Z (single layered AFM), at a volume of 10.81 Å^3 with $c/a = 1.08$. The energy landscape around this minimum, however, is quite flat along all parameters (i.e., with respect to changes in volume, c/a ratio, and propagation vector), and there is again a multitude of structure/spin configurations which can be considered to be degenerate. The energy difference between aforementioned equilibrium configuration(s) of fct-Fe and the equilibrium structure(s) of fcc-Fe, however, is quite substantial (see Table IV). A comparison with the study of collinear magnetic configurations in fct-Fe by Spišák *et al.*[35] indicates that a bilayer antiferromagnetic configuration [equivalent to a spin-density wave with $\vec{q} = 2\pi/a \times (0,0,0.5)$], which we did not include in the present study, is probably even lower in energy than the spin-spiral solution at $(10.81, 1.08, Z)$.

Orthorhombic distortions. In the case of orthorhombic distortions of the fct structure, we limited our search through the $(\Omega, c/a, b/a, \vec{q})$ parameter space to the optimization of c/a and b/a for spin-spiral configurations near $\vec{q}_2$, at volumes below 11.00 Å^3. For $\Omega < 10.72$ Å^3, small orthorhombic distortions ($b/a \approx 1.02$) stabilize the spin-spiral solution at $\vec{q}_2$ over the solution at Z, although the energy differences involved are very small. The equilibrium configuration of the fct structure, i.e., $\Omega = 10.81$ Å^3 with $c/a = 1.08$ and $\vec{q} = Z$, however, is stable against orthorhombic distortions.

Monoclinic shearing. We have studied the stability against monoclinic shearing for the three (local) minima in the $(\Omega, c/a, \vec{q})$ parameter space of the fct structures: (i) FM, $\Omega = 11.69$ Å^3 with $c/a = 1.18$ and $\vec{q} = \Gamma$, (ii) SS, $\Omega = 11.18$ Å^3 with $c/a = 1.10$ and $\vec{q} = \vec{q}_1$, and (iii) AFM, $\Omega = 10.81$ Å^3 with $c/a = 1.08$ and $\vec{q} = Z$. Monoclinic shearing strongly lowers the energy of spin-spiral solutions near Γ in all three structures, and for $\delta \approx 0.35$ all three are predicted to order ferromagnetically. Especially structure (i), the equilibrium fct structure in case of ferromagnetic ordering is affected by monoclinic shearing. For $\delta = 0.35$, the ferromagnetic solution in structure (i) is almost 80 meV, and more than 100 meV, lower in energy than the equilibrium configuration(s) of the fct and fcc structures, respectively (see Table IV). This solution ($\Omega = 11.69$ Å^3, $c/a = 1.18$, $\delta = 0.35$, $\vec{q} = \Gamma$) has the lowest total energy of all structures considered in the present work. It compares quite favorably with the calculations of Ref. 37 where an extensive optimization of Ω, c/a, and δ, for monoclinically sheared fct-Fe in the ferromagnetic state yielded an equilibrium structure given by $\Omega = 11.50$ Å^3, $c/a = 1.17$, and $\delta = 0.33$ (see Table II). Both other structures we considered, (ii) and (iii), show the same instability against monoclinic shearing in the ferromagnetic state, as was found for structure (i). The fact that our calculations predict a value of $\delta \approx 0.35$ for all three structures, at $\vec{q} = \Gamma$, shows the shearing instability in case of ferromagnetic ordering to be more or less independent from the other structural parameters, volume and c/a ratio. In combination with

the observation that for propagation vectors away from Γ, monoclinic shearing either lowers the total energy to a much smaller extend than at $\vec{q} = \Gamma$, or raises it (see Figs. 11 and 12), we are confident that a more thorough search through the $(\Omega, c/a, \delta, \vec{q})$ parameter space will not yield a different equilibrium configuration for monoclinically sheared fct-Fe.

VII. CONCLUSIONS

We have investigated the influence of broken crystalline and magnetic symmetries on the stability of fcc (or near fcc) γ-Fe. We find that when the crystal structure is constrained to cubic symmetry, the magnetic ground state is indeed a spin-spiral with a propagation vector $\vec{q}_2 = 2\pi/a \times (0.2, 0, 1)$ very close to the propagation vector determined experimentally. The problematic point is that the atomic volume at which this global minimum is found is considerably lower than the atomic volume of γ-Fe precipitates in a Cu matrix, on which the experiments have been performed. At these larger volumes, the magnetic state predicted by the calculations is a spin spiral with $\vec{q}_1 = 2\pi/a \times (0, 0, 0.6)$. The tendency of even the most accurate GGA calculations to underestimate the equilibrium volume of the most stable magnetic configurations of the itinerant magnets close to the AFM/FM transition (i.e., Fe and Mn) seems to be a general shortcoming of current LSD theory, for α-Mn as well, the atomic volume at which the complex noncollinear magnetic state is in equilibrium is underestimated compared to experiment.[6]

When a broken cubic symmetry is admitted, we find that tetragonal distortions stabilize the spin spiral with $\vec{q}_1$ over the one with $\vec{q}_2$. At large distortions, however, a commensurate AFM state is stabilized at low volumes, and a FM high-spin state at larger volumes.

Orthorhombic distortions change this picture only marginally, but monoclinic shear deformation has a dramatic influence on the stability of the competing magnetic configurations: spin-spiral states are generally disfavored—this is not surprising since the lowering of the crystalline symmetry is to some degree incompatible with a helical symmetry of the magnetization density along a preferred axis. Even more importantly, we find that a monoclinic shear deformation stabilizes a ferromagnetic state and that in all phases the strength of the monoclinic distortions and the partially ferromagnetic character are directly correlated.

Together, our results provide a convincing explanation of the widely differing structural and magnetic properties of γ-Fe stabilized by either the three-dimensional embedding in an fcc matrix or the epitaxial constraint in ultrathin films. In γ-Fe precipitates, only very small deviations from cubic symmetry are admitted. In this case the magnetic ground state is a spin spiral. The small deviations from cubic symmetry could eventually tip the balance between the almost degenerate spin-spiral states. In ultrathin films, the fundamental instability of γ-Fe against both tetragonal and monoclinic distortions leads to the formation of nanodomains of

monoclinically sheared FM Fe (for film thicknesses up to 4 ML) or biAFM Fe, in thicker films, as observed in STM experiments. The observed geometry in these domains agrees quantitatively with that deduced from our calculations. Our new results demonstrate that these structural distortions suppress the formation of spin-spiral states in ultrathin films. Hence precipitates and ultrathin films must be considered as two different phases of γ-Fe.

[1] W. Hume-Rothery, *Electrons, Atoms, Metals, and Alloys*, 3rd ed. (Dover, New York, 1963), p. 251.

[2] N. Saito, H. Hiroyoshi, K. Fukamichi, and Y. Nakagawa, J. Phys. F: Met. Phys. **16**, 911 (1986).

[3] D.H. Ryan, J.M.D. Coey, E. Batalla, Z. Altounian, and J.O. Ström-Olsen, Phys. Rev. B **35**, 8630 (1987).

[4] R. Lorenz and J. Hafner, J. Magn. Magn. Mater. **139**, 209 (1995).

[5] A.C. Lawson, A.C. Larson, M.C. Aronson, S. Johnson, Z. Fisk, P.C. Canfield, J.D. Thompson, and R.B. Von Dreele, J. Appl. Phys. **76**, 7049 (1994).

[6] D. Hobbs and J. Hafner, J. Phys.: Condens. Matter **13**, L681 (2001).

[7] Y. Endoh and Y. Ishikawa, J. Phys. Soc. Jpn. **30**, 1614 (1971).

[8] T. Oguchi and A.J. Freeman, J. Magn. Magn. Mater. **46**, L1 (1984).

[9] H. Zabel, J. Phys.: Condens. Matter **11**, 9303 (1999).

[10] R. Hafner, D. Spišák, R. Lorenz, and J. Hafner, J. Phys.: Condens. Matter **13**, L239 (2001).

[11] Y. Tsunoda and N. Kunitomi, Solid State Commun. **54**, 547 (1985).

[12] Y. Tsunoda, N. Kunitomi, and R.M. Nicklow, J. Phys. F: Met. Phys. **17**, 2447 (1987).

[13] Y. Tsunoda and N. Kunitomi, J. Phys. F: Met. Phys. **18**, 1405 (1988).

[14] Y. Tsunoda, S. Imada, and N. Kunitomi, J. Phys. F: Met. Phys. **18**, 1421 (1988).

[15] Y. Tsunoda, J. Phys.: Condens. Matter **1**, 10 427 (1989).

[16] Y. Tsunoda, J. Phys. Soc. Jpn. **58**, 1648 (1989).

[17] Y. Tsunoda, J. Phys.: Condens. Matter **3**, 7231 (1991).

[18] B.T. Jonker, K.H. Walker, E. Kisker, G.A. Prinz, and C. Carbone, Phys. Rev. Lett. **57**, 142 (1986).

[19] W.A.A. Macedo and W. Keune, Phys. Rev. Lett. **61**, 475 (1988).

[20] H. Magnan, D. Chandesris, B. Villette, O. Heckmann, and J. Lecante, Phys. Rev. Lett. **67**, 859 (1991).

[21] J. Thomassen, F. May, B. Feldmann, M. Wuttig, and H. Ibach, Phys. Rev. Lett. **69**, 3831 (1992).

[22] S. Müller, P. Bayer, C. Reischl, K. Heinz, B. Feldmann, H. Zillgen, and M. Wuttig, Phys. Rev. Lett. **74**, 765 (1995).

[23] R.D. Ellerbrock, A. Fuest, A. Schatz, W. Keune, and R.A. Brand, Phys. Rev. Lett. **74**, 3053 (1995).

[24] D.J. Keavney, D.F. Storm, J.W. Freeland, I.L. Grigorov, and J.C. Walker, Phys. Rev. Lett. **74**, 4531 (1995).

[25] M. Straub, R. Vollmer, and J. Kirschner, Phys. Rev. Lett. **77**, 743 (1996).

[26] D. Qian, X.F. Jin, J. Barthel, M. Klaua, and J. Kirschner, Phys. Rev. Lett. **87**, 227204 (2001).

[27] A. Biedermann, M. Schmid, and P. Varga, Phys. Rev. Lett. **86**, 464 (2001).

[28] J. Giergiel, J. Shen, J. Woltersdorf, A. Kirilyuk, and J. Kirschner, Phys. Rev. B **52**, 8528 (1995).

[29] W. Pitsch, Philos. Mag. **4**, 577 (1959).

[30] E.G. Moroni, J. Hafner, and G. Kresse, J. Phys.: Condens. Matter **1**, L35 (1999).

[31] V.L. Moruzzi, P.M. Marcus, and J. Kübler, Phys. Rev. B **39**, 6957 (1989).

[32] T. Kraft, P.M. Marcus, and M. Scheffler, Phys. Rev. B **49**, 11 511 (1994).

[33] R. Lorenz and J. Hafner, Thin Solid Films **281**, 492 (1996); Phys. Rev. B **54**, 15 937 (1996).

[34] T. Asada and S. Blügel, Phys. Rev. Lett. **79**, 507 (1997).

[35] D. Spišák and J. Hafner, Phys. Rev. B **61**, 16 129 (2000).

[36] S.L. Qiu, P.M. Marcus, and Hong Ma, Phys. Rev. B **62**, 3292 (2000).

[37] D. Spišák and J. Hafner, Phys. Rev. Lett. **88**, 056101 (2002).

[38] D. Spišák and J. Hafner (unpublished).

[39] D. Spišák and J. Hafner, Phys. Rev. B **56**, 2646 (1997).

[40] O.N. Mryasov, A.I. Lichtenstein, L.M. Sandratskii, and V.A. Gubanov, J. Phys.: Condens. Matter **3**, 7683 (1991).

[41] M. Uhl, L.M. Sandratskii, and J. Kübler, J. Magn. Magn. Mater. **103**, 314 (1992).

[42] V.P. Antropov, M.I. Katsnelson, B.N. Harmon, M. van Schilfgaarde, and D. Kusnezov, Phys. Rev. B **54**, 1019 (1996); V.P. Antropov, M.I. Katsnelson, M. van Schilfgaarde, and B.N. Harmon, Phys. Rev. Lett. **75**, 729 (1995).

[43] M. Körling and J. Ergon, Phys. Rev. B **54**, 8293 (1993).

[44] D.M. Bylander and L. Kleinman, Phys. Rev. B **60**, 9916 (1999).

[45] P. James, O. Eriksson, B. Johansson, and I.A. Abrikosov, Phys. Rev. B **59**, 419 (1999).

[46] H.C. Herper, E. Hoffmann, and P. Entel, Phys. Rev. B **60**, 3839 (1999).

[47] K. Knöpfle, L.M. Sandratskii, and J. Kübler, Phys. Rev. B **62**, 5564 (2000).

[48] S.J. Luo and K.L. Yao, Solid State Commun. **120**, 233 (2001).

[49] G. Kresse and J. Hafner, Phys. Rev. B **48**, 13 115 (1993).

[50] G. Kresse and J. Furthmüller, Phys. Rev. B **54**, 11 169 (1996); Comput. Mater. Sci. **6**, 15 (1996).

[51] D. Hobbs, G. Kresse, and J. Hafner, Phys. Rev. B **62**, 11 556 (2000).

[52] C. Herring in *Magnetism*, edited by G. T. Rado and H. Suhl (Academic Press, New York, 1966).

[53] L.M. Sandratskii, J. Phys.: Condens. Matter **3**, 8565 (1993); **3**, 8587 (1993).

[54] P.E. Blöchl, Phys. Rev. B **50**, 17 953 (1994).

[55] G. Kresse and D. Joubert, Phys. Rev. **59**, 1758 (1999).

[56] J.P. Perdew, K. Burke, and M. Ernzerhof, Phys. Rev. Lett. **77**, 3865 (1996).

[57] S.H. Vosko, L. Wilk, and M. Nusair, Can. J. Phys. **58**, 1200 (1980).

[58] J.P. Perdew and A. Zunger, Phys. Rev. B **23**, 5048 (1981).

[59] J.P. Perdew, J.A. Chevary, S.H. Vosko, K.A. Jackson, M.R. Pederson, D.J. Singh, and C. Fiolhais, Phys. Rev. B **46**, 6671 (1992).

[60] H.J. Monkhorst and J.D. Pack, Phys. Rev. B **13**, 1588 (1976).

[61] P.E. Blöchl, O. Jepsen, and O.K. Andersen, Phys. Rev. B **49**, 16 223 (1994).

[62] M. Körling and J. Ergon, Physica B **237−238**, 353 (1997).